第34卷 第6期 焊 接 学 报 Vol. 34 No. 6
2013年6月 TRANSACTIONS OF THE CHINA WELDING INSTITUTION June 2013

盲孔法测量非均匀残余应力时的释放系数

李 昊，李 华
（合肥工业大学 土木与水利工程学院，合肥 230009）

李 昊

摘 要：盲孔法测量沿深度非均匀的残余应力时，积分法是最常用的计算方法，其释放系数矩阵 $[a]$，$[b]$ 对计算精度有很大影响. 由于在标定释放系数矩阵时假定各层上的残余应力均匀分布，当应力梯度变化较大时会引起较大的计算误差. 文中首先建立了标定释放系数矩阵的三维有限元模型，并通过模拟均匀残余应力场验证了其有效性. 在此基础上分析了积分法标定的释放系数矩阵用于计算沿深度非均匀残余应力时的误差，并提出了二次标定的修正方法. 结果表明，采用二次标定的释放系数矩阵计算得到的残余应力值更接近于真实应力.

关键词：盲孔法；非均匀残余应力；积分法；释放系数；二次标定
中图分类号：TG404 **文献标识码**：A **文章编号**：0253－360X(2013)06－0085－04

0 序 言

释放系数的确定是盲孔法测量残余应力的关键一环，目前在确定释放系数时均假定残余应力沿深度方向均匀分布，并在已知均匀应力场中标定释放系数[1－5]. 然而在实际结构中，特别是焊接结构的焊缝附近，残余应力沿深度方向通常为非均匀分布，而且变化梯度较大. 此时如果依然使用均匀场中所标定出的释放系数进行计算，势必会产生较大的误差. 为了解决这一问题，Schajer[6,7] 考虑了相同深度上的残余应力在不同孔深时应力释放所产生的应变，提出了积分计算方法，为盲孔法测量沿深度非均匀的残余应力提供了理论基础. 但是该方法在对每层上的释放系数进行标定时，仍假定该层上的残余应力沿深度方向均匀分布，这与真实情况仍不符合. 为此文中采用有限元方法，分析应用积分法的释放系数计算沿深度非均匀变化的残余应力时的误差，并提出相应的修正方法.

1 积分法及其修正方法

1.1 积分法的基本原理

Schajer[6,7] 提出的积分法的基本思想是通过逐层钻孔将构件不同深度上的残余应力逐步释放，同时测量每次钻孔后的表面释放应变，并认为每次测得的表面释放应变不仅是由该层深度的残余应力释放引起的，而且还包括前几次钻孔深度上的残余应力进一步释放的结果. 因而不同深度上的残余应力与表面释放应变的关系为

$$\left.\begin{aligned}[a]\{P\} &= E\{m\}/(1+\mu)\\ [b]\{Q\} &= E\{q\}\\ [b]\{T\} &= E\{t\}\end{aligned}\right\} \tag{1}$$

式中：E 和 μ 分别为弹性模量和泊松比；向量 $\{P\}$，$\{Q\}$ 和 $\{T\}$ 中的元素 P_i，Q_i 和 T_i，分别为第 i 层深度的应力，且 $P_i=(\sigma_{xi}+\sigma_{yi})/2$，$Q_i=(\sigma_{xi}-\sigma_{yi})/2$，$T_i=\tau_{xyi}$，其中 σ_{xi} 和 σ_{yi} 分别为第 i 层深度上 x 方向和 y 方向的正应力，τ_{xyi} 为此深度的切应力；向量 $\{m\}$，$\{q\}$ 和 $\{t\}$ 中的元素 m_i，q_i 和 t_i 分别为第 i 次钻孔时的表面应变，且 $m_i=(\varepsilon_{1i}+\varepsilon_{3i})/2$，$q_i=(\varepsilon_{1i}-\varepsilon_{3i})/2$，$t_i=(\varepsilon_{1i}+\varepsilon_{3i}-2\varepsilon_{2i})/2$，其中 ε_{1i}，ε_{2i}，ε_{3i} 为第 i 次钻孔时3个方向的表面释放应变；释放系数矩阵 $[a]$，$[b]$ 为下三角矩阵，其元素 a_{ij}，b_{ij} 表示第 i 次钻孔时，第 j 层深度上单位应力释放所产生的表面释放应变. 由此可求得第 i 层深度上残余应力的主应力 σ_{1i} 和 σ_{2i} 为

$$\sigma_{1i},\sigma_{2i}=P_i\pm\sqrt{Q_i^2+T_i^2} \tag{2}$$

积分法中释放系数矩阵的定义与常规方法有较大区别，以释放系数矩阵 $[a]$ 为例，其元素为各层深度上施加单位应力时对应的释放应变. 图1给出了4次钻孔时矩阵 $[a]$ 中各元素的确定方法. 由图1可以看出，确定释放系数矩阵时，需要在孔壁上分层施加均匀载荷，这种加载方式难以实现. 因而释放

收稿日期：2012－05－09

系数矩阵通常采用数值模拟的方法来进行标定.

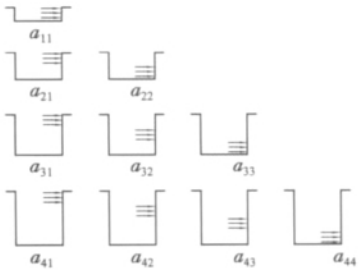

图 1 矩阵 [a] 中元素 a_{ij} 所对应的残余应力

Fig. 1 Residual stresses corresponding to coefficients a_{ij} of matrix [a]

1.2 修正方法

由上文可以看出,积分法标定释放系数矩阵时,仍然假定各层上的残余应力均匀分布,当应力梯度变化较大时,会引起较大的计算误差. 为此提出了对释放系数矩阵进行二次标定的修正方法. 首先根据积分法计算出各层深度上的残余应力,并运用最小二乘法拟合出残余应力沿深度方向的分布曲线,然后根据拟合所得应力对释放系数矩阵进行重新标定,并采用二次标定的释放系数矩阵重新计算各层深度上的残余应力. 图 2 为 4 次钻孔时释放系数矩阵 [a] 二次标定的示意图,图 2 中孔壁上分层施加的应力为拟合后的应力.

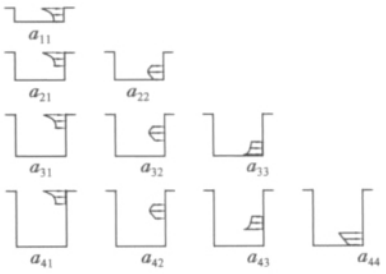

图 2 矩阵 [a] 的二次标定

Fig. 2 Recalibration of matrix [a]

2 数值模拟

2.1 释放系数矩阵的标定

采用有限元分析软件 ANSYS 进行建模,模型大小为 100 mm × 50 mm × 8 mm,假定材料的弹性模量 $E = 210$ GPa,泊松比 $\mu = 0.3$. 选取 ASTM 标准中平均直径 $D = 2.57$ mm 的 A 型应变花[1] 进行数值模拟,盲孔直径为 $0.4D$. 模拟 4 次钻孔,每次钻孔增量为 $0.05D$. 为了提高有限元模型求解的精度,在应变片对应位置处按照应变片的实际大小和形状划分网格,盲孔附近的网格划分如图 3 所示. 将所有单元的平均应变作为应变片的测量应变,获得的释放系数矩阵 [a] 和 [b] 分别为

$$[a] = \begin{bmatrix} -0.048\ 363 & & & \\ -0.067\ 860 & -0.041\ 500 & & \\ -0.077\ 808 & -0.052\ 781 & -0.024\ 909 & \\ -0.082\ 147 & -0.058\ 116 & -0.031\ 581 & -0.011\ 032 \end{bmatrix} \tag{3}$$

$$[b] = \begin{bmatrix} -0.089\ 025 & & & \\ -0.119\ 352 & -0.084\ 314 & & \\ -0.133\ 287 & -0.107\ 680 & -0.063\ 561 & \\ -0.139\ 265 & -0.118\ 239 & -0.075\ 233 & -0.042\ 160 \end{bmatrix} \tag{4}$$

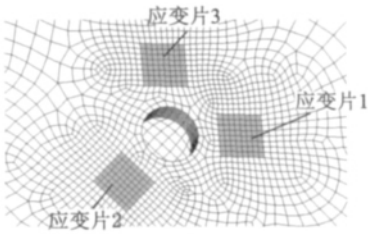

图 3 盲孔附近的网格划分

Fig. 3 Mesh near blind hole

为了验证有限元模型以及数值模拟标定的有效性,采用模拟得到的释放系数矩阵计算一个已知均匀残余应力场. 模型尺寸、材料属性、应变花型号、钻孔次数、孔径和孔深均与标定时相同. 模型长边和短边施加的压力分别为 $p_1 = 100$ MPa,$p_2 = -50$ MPa. 将含孔模型和无孔模型所得到的测量应变之差,作为每次钻孔深度下的释放应变,4 次钻孔深度下的释放应变 ε_1,ε_2,ε_3 如表 1 所示.

表 1 均匀场下的释放应变

Table 1 Relieved strains in uniform stress field

孔深 h/mm	释放应变 ε_{pi}/(μm·m^{-1})		
	ε_{p1}	ε_{p2}	ε_{p3}
0.128 5	−41.77	−7.28	27.21
0.257 0	−88.79	−16.44	55.93
0.385 5	−132.34	−23.45	85.48
0.514 0	−162.42	−27.56	107.30

将释放系数矩阵 [a],[b] 和表 1 中的释放应变代入式(1)和式(2),可以计算出每次钻孔深度下的主应力值,计算结果如图 4 所示. 从图 4 中可以看

出,残余应力沿深度均匀分布时,由数值模拟的释放系数矩阵计算得到的应力值与真实应力值相差很小. 这说明了标定的有限元模型及其释放系数矩阵是可靠的.

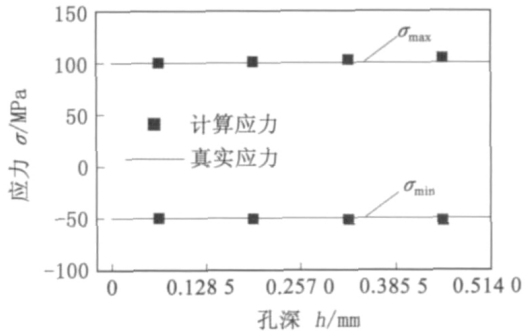

图 4　模拟计算结果与真实值的比较

Fig. 4　Comparison of simulated results with real ones

2.2　非均匀场的数值模拟计算

构造沿孔深线性分布和二次函数分布的双向等值应力场 σ_1 和 σ_e,其表达式分别为

$$\sigma_1 = -1\,274.3h + 412.05$$

$$\sigma_e = 787.3h^2 - 432h + 34.4 \qquad (5)$$

式中: h 为孔深. 有限元模型尺寸、材料属性、应变花型号、钻孔次数、孔径和孔深均与上节相同. 将构造的残余应力场分别加载到有限元模型上,得到的两种应力场下的释放应变如表 2 所示. 将前文得到的释放系数矩阵 [a], [b] 和表 2 中的释放应变代入式(1)和式(2),可求得 4 次钻孔深度下的残余应力值,并与真实值进行比较,结果如表 3 所示. 从表 3 中可以看出,对于沿深度非均匀的残余应力场,积分法采用均匀应力标定的释放系数矩阵所求得的残余应力值与真实应力之间存在较大误差.

表 2　非均匀场下的释放应变

Table 2　Relieved strains in non-uniform stress field

孔深 h/mm	线性场的释放应变 $\varepsilon_{1i}/(\mu m\cdot m^{-1})$			二次函数的释放应变 $\varepsilon_{ei}/(\mu m\cdot m^{-1})$		
	ε_{11}	ε_{12}	ε_{13}	ε_{e1}	ε_{e2}	ε_{e3}
0.128 5	−98.24	−98.24	−98.22	−3.66	−3.66	−3.66
0.257 0	−181.37	−181.37	−181.36	−0.52	−0.52	−0.52
0.385 5	−215.55	−215.55	−215.53	3.70	3.70	3.70
0.514 0	−219.17	−219.16	−219.15	5.09	5.09	5.08

将表 3 中积分法计算应力值进行最小二乘法拟合,拟合得到的非均匀应力分段施加到标定模型上,按照 1.2 节所述修正方法对 4 次钻孔深度上的释放

表 3　残余应力积分法计算值与真实值的比较

Table 3　Comparison of calculated values by integral method with real ones

孔深 h/mm	线性应力 σ_1/MPa			二次函数应力 σ_e/MPa		
	真实应力 $\tilde{\sigma}_1$	积分法计算值 $\hat{\sigma}_1$	误差 δ_1(%)	真实应力 $\tilde{\sigma}_e$	积分法计算值 $\hat{\sigma}_e$	误差 δ_e(%)
0.064 25	330.2	336.9	2.03	9.5	12.6	32.63
0.192 75	166.4	174.0	4.57	−20.0	−18.5	7.50
0.321 25	2.7	14.4	433.33	−23.5	−24.7	5.11
0.449 75	−161.1	−171.3	6.33	−1.0	−1.9	90.00

系数矩阵进行二次标定,再运用二次标定的释放系数矩阵重新计算相应深度的残余应力,其结果如表 4 所示. 从表 4 中可知,采用二次标定后的释放系数矩阵计算得到的残余应力值更接近真实应力.

表 4 残余应力修正法计算值与真实值的比较

Table 4　Comparison of calculated values by improvement method with real ones

孔深 h/mm	线性应力 σ_1/MPa			二次函数的应力 σ_e/MPa		
	真实应力 $\tilde{\sigma}_1$	修正法计算值 $\hat{\sigma}_1$	误差 $\hat{\delta}_1$(%)	真实应力 $\tilde{\sigma}_e$	修正法计算值 $\hat{\sigma}_e$	误差 $\hat{\delta}_e$(%)
0.064 25	330.2	330.2	0	9.5	10.9	14.74
0.192 75	166.4	166.5	0.06	−20.0	−19.4	3.00
0.321 25	2.7	3.8	40.74	−23.5	−22.4	4.68
0.449 75	−161.1	−162.8	1.06	−1.0	−0.8	20.00

3　试验验证

采用文献 [8] 中所得到的 4 点弯曲梁试验数据来进一步验证修正方法的有效性. 试验中所采用的钢梁尺寸为 400 mm × 100 mm × 12.5 mm,材料的弹性模量为 $E = 209.4$ GPa,泊松比为 $\mu = 0.27$. 通过加载使钢梁产生塑性变形,从而在内部产生一个沿梁厚度方向线性变化的残余应力场,其分布如图 5 所示. 梁表面的最大残余应力 $\sigma_A = \pm 130$ MPa,内部的最大残余应力 $\sigma_B = \pm 133$ MPa. 试验选用的应

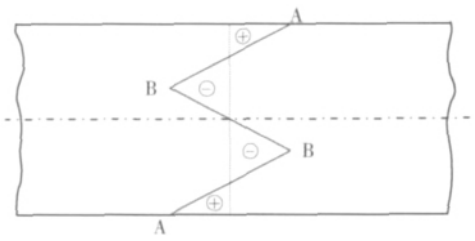

图 5　梁中残余应力的分布

Fig. 5　Distribution of residual stress in beam

变花型号为 MM-EA-06-125RE-120，钻孔直径为 3.078 mm，钻孔总深度为 2.6 mm，每次钻孔深度增量为 0.1 mm. 文中选取钻孔深度分别为 0.5，1.0，1.5，2.0 mm 时的释放应变进行计算，其数据及两种方法的计算结果如表 5 和表 6 所示.

表 5 试验中的释放应变

Table 5 Relieved strains in test

孔深 h/mm	释放应变 ε_{ti}/($\mu m \cdot m^{-1}$)		
	ε_{t1}	ε_{t2}	ε_{t3}
0.5	4	−8	−22
1.0	9	−22	−43
1.5	13	−28	−57
2.0	19	−25	−63

表 6 两种方法计算的残余应力值的比较

Table 6 Comparison between residual stresses calculated by two methods

孔深 h/mm	真实应力 $\tilde{\sigma}_t$/MPa	积分法计算值 $\hat{\sigma}_t$/MPa	修正法计算值 $\hat{\sigma}_t$/MPa	积分法误差 $\hat{\delta}_t$(%)	修正法误差 $\hat{\delta}_t$(%)
0.25	111.74	120.91	112.97	8.21	1.10
0.75	75.22	82.52	76.67	9.70	1.93
1.25	38.71	43.26	39.98	11.75	3.28
1.75	2.19	6.43	1.73	193.61	21.00

由表 6 可以看出，运用修正方法所计算出的残余应力更为贴近真实应力值.

4 结 论

(1) 采用均匀场标定得到的释放系数矩阵计算沿深度方向均匀分布的残余应力时较为准确，但是用于非均匀残余应力场的计算会产生较大的误差.

(2) 采用文中提出的修正方法，运用二次标定的释放系数矩阵计算沿深度方向非均匀分布的残余应力，其计算结果与真实应力的偏差较小，修正结果令人满意，从而提高了测量精度.

参考文献:

[1] ASTM. Determining residual stresses by the hole-drilling strain-gage method [S]. Philadelphia: American Society for Testing and Materials, 1995.

[2] 陆才善. 残余应力测试小孔释放法 [M]. 西安: 西安交通大学出版社, 1991.

[3] 陈怀宁，陈亮山，董秀中. 盲孔法测量残余应力的钻削加工应变 [J]. 焊接学报, 1994, 15(4): 276 − 279.
Chen Huaining, Chen Liangshan, Dong Xiuzhong. Drilling strains in measuring residual stress with hole-drilling strain-gage method [J]. Transactions of the China Welding Institution, 1994, 15(4): 276 − 279.

[4] 李 昊，刘一华. 钻孔法中的残余应力场 I 理论分析 [J]. 焊接学报, 2008, 29(9): 46 − 50.
Li Hao, Liu Yihua. Residual stress field in hole-drilling method part I: theoretical analysis [J]. Transactions of the China Welding Institution, 2008, 29(9): 46 − 50.

[5] 马雯波，陈曙光，刘荟琼，等. 盲孔法中应变释放系数的有限元模拟标定 [J]. 焊接学报, 2011, 32(2): 97 − 100.
Ma Wenbo, Chen Shuguang, Liu Huiqiong, *et al*. FEM simulation of calibration on strain release coefficients in blind hole method [J]. Transactions of the China Welding Institution, 2011, 32(2): 97 − 100.

[6] Schajer G S. Measurement of non-uniform residual stresses using the hole-drilling method Part I: stress calculation procedures [J]. Journal of Engineering Materials and Technology, 1988, 110(4): 338 − 343.

[7] Schajer G S. Measurement of non-uniform residual stresses using the hole-drilling method Part II: practical application of the integral method [J]. Journal of Engineering Materials and Technology, 1988, 110(4): 344 − 349.

[8] Petrucci G, Zuccarello B. A new calculation procedure for non uniform residual stress analysis by the hole-drilling method [J]. The Journal of Strain Analysis for Engineering Design, 1998, 33(1): 27 − 37.

作者简介：李 昊，男，1971 年出生，博士，副教授，硕士研究生导师. 主要从事残余应力分析与测试、复合材料等方面的科研工作. 发表论文 30 余篇. Email: lhtwd@sina.com

pp 73 – 76

Abstract: 7075-T6 aluminum alloy was successfully spot joined by refill friction stir spot welding process. The microstructure, microhardness, tensile/shear strength and cross-tension strength of the joints were tested. Experimental results indicate that the microstructure can be divided into the nugget zone, thermo-mechanically affected zone, heat-affected zone and base material, respectively. Defects such as hook, cavity, incomplete fusion, incomplete refill and bonding ligament were found in the joint. The microhardness profile in the welded zone exhibited W-shaped appearance, but that in the stir zone exhibited V-shaped appearance. When the rotational speed was 1 400 r/min, the highest tensile/shear strength reached 7 916.0 N, which was 39.6% of the base material. The change of the cross-tension strength with the processing parameters was complicated, and the highest cross-tension strength can reach 43.9 MPa.

Key words: aluminum alloy; friction spot welding; microstructure; mechanical property

Effect of precoating on microstructure of SiC reinforced iron-based coating GAO Zhen, DU Xiaodong, WANG Jinjia, SONG Zili (School of Materials Science and Engineering, Hefei University of Technology, Hefei 230009, China). pp 77 – 80

Abstract: The reaction layers consisting of Cr_3Si, Cr_7C_3 and $Cr_{23}C_6$ were produced on SiC surface by PIRAC technology. The iron-based alloy coating reinforced by precoated SiC particles was prepared by plasma surfacing process with the back-feeding model. The results show that the non-precoated SiC particles dissolve completely in the coating. Massive primary polygonal carbides formed in the upper part, dendrites formed in the middle part and cellular grains generated in the bottom part. The precoated SiC particles distributed in the coating surface, retaining the original shape, and did not dissolve significantly. The region between SiC particles and the matrix could be divided into the interface reaction zone and the transition zone. The interface reaction zone consisted of α-(Fe,Cr) solid solution, massive $(Fe,Cr)_7C_3$ and $(Fe,Cr)_{23}C_6$ carbides. The transition zone consisted of the α-(Fe,Cr) solid solution with high Cr content, and it was difficult to expose the microstructure due to its excellent corrosion resistance.

Key words: SiC; precoating; microstructure; interface reaction

Analysis of orthogonal test of properties of dual-phase DP600 steel resistance spot welded joint TAO Bohao[1], LI Hong[1], SONG Yonglun[2], LI Qiang[2] (1. School of Materials Science and Engineering, Beijing University of Technology, Beijing 100124, China; 2. School of Mechanical Engineering and Applied Electronics Technology, Beijing University of Technology, Beijing 100124, China). pp 81 – 84

Abstract: The spot welding parameters for cold-rolled dual-phase DP600 steel in industrial trial production were optimized by orthogonal experimental design method with the tensile/shear loads of spot welded joints as the evaluation index. The welding window and optimal welding parameters were achieved by range analysis and variance analysis. The microstructure and tensile/shear loads of the spot welded joints under optimized welding parameters were investigated. The results showed that the welding current was between 9 000 A and 12 000 A, and the welding time was between 200 ms and 500 ms in the welding window. The welding current had most remarkable influence on the joint strength. With the increase of welding current, the tensile/shear loads increased. The maximum load 14 kN and the maximum absorbing energy 45.26 kJ were obtained with 12 000 A welding current, 200 ms welding time and 2 500 N electrode pressure. And the microstructure of the resultant welded nugget mainly consisted of lath martensite.

Key words: resistance spot welding; DP600 steel; orthogonal experiment design; range analysis; variance analysis

Release coefficients during measuring non-uniform residual stress with blind-hole method LI Hao, LI Hua (School of Civil and Hydraulic Engineering, Hefei University of Technology, Hefei 230009, China). pp 85 – 88

Abstract: Integral method is widely used in calculating the non-uniform residual stresses from the measured relaxed strains using the blind-hole method, in which the release coefficients have great influence on the measurement accuracy. As the residual stresses in each layer are assumed to be uniform when calibrating the coefficients, the calculated results are considerably different from the real stresses if the residual stresses vary rapidly along the depth. In this paper, a three-dimensional FEM model was established for the release coefficients, and verified by a simulated test on a uniform loaded plate. The errors in the calculation of the non-uniform residual stress field were studied using the release coefficients calibrated by the integral method, and then an improved technique was proposed to recalibrate the release coefficients. The results show that the calculated residual stresses using the recalibrated coefficients are closer to the real ones.

Key words: blind-hole method; non-uniform residual stress; integral method; release coefficient; recalibration

Finite element simulation of rectifying roundness of welded thin-walled cylinder by extrusion LI Jun[1,2], ZHANG Wenfeng[1], FANG Hongyuan[2] (1. Zhejiang Yinlun Machinery Company Ltd., Tiantai 317200, China; 2. State Key Laboratory of Advanced Welding and Joining, Harbin Institute of Technology, Harbin 150001, China). pp 89 – 92

Abstract: The method of rectifying the roundness of welded thin-walled cylinders was proposed by extruding the metal in and around the weld. The effect of roundness rectification by extrusion and the mechanism in which the effect lies were investigated by finite element method (FEM). The cylinder welded longitudinally has a peach shape in radial direction and significantly distorts at two ends. The simulation results show that the extrusion method can effectively improve the roundness of the welded cylinder. The effectiveness of rectifying the roundness of welded thin-walled cylinders by extrusion was verified with self-made devices. The experimental results show that the roundness at the ends of welded stainless steel cylinders with 2 mm in wall thickness, 300 mm in length and 280 mm in external diameter can be reduced to about 0.5 mm by extruding the metal in and around the weld.

Key words: welding; thin wall; cylinder; extrusion; numerical simulation

Effect of crack location on limit loads of strength mismatched welded joints DUAN Xiaoxue[1], ZHANG Yanhua[1], XIONG Linyu[2], TIAN Zhijie[2], SU Zhiqiang[2] (1. School of Mechanical Engineering and Automation, Beihang University, Beijing 100191,